

Effect of Structural, Electrical, and Magnetic properties of Nano-sized $\text{Mg Er}_x \text{Dy}_y \text{Fe}_{2-x-y} \text{O}_4$

Vasant Naidu¹, Sindhu Chandra², K.S.P.Durairaj³,
Jeyaperumal Kalyana Sundar⁴ and M.Sivabharathy*³

¹Department of ECE, Sethu Institute of Technology, Kariapatti- 626 115, India

²Consultant, gynaecologist Corniche Hospital, Abu Dhabi, UAE

³Department of Physics, Sethu Institute of Technology, Kariapatti- 626 115, India

⁴Department of Physics, Periyar University, Salem - 636 011, India

*Corres.author : msbsivabharathy@yahoo.co.in

Abstract: The realization of nano-sized, highly-featured, Magnesium Erbium Dysprosium Ferrite ($\text{Mg Er}_x \text{Dy}_y \text{Fe}_{2-x-y} \text{O}_4$) for the preparation of microstrip patch(MSP)antenna substrates is being reported in this present investigation. The structural, electrical, magnetic measurements were made to characterize these as-prepared particles. This composite showed an increase in the permittivity, dc resistivity and reduction in relative loss factor. These values were large enough as compared with MgFe_2O_4 , $\text{MgEr}_x\text{Fe}_{2-x}\text{O}_4$, $\text{MgDy}_y\text{Fe}_{2-y}\text{O}_4$. The decreasing magnetostriction constant and increasing in densification due to Er and Dy substitution caused the change in conduction mechanism due to the increase in the drift mobility of the thermally activated electrons as the main source for the hopping conducting mechanism. This causes an increase in permittivity. These results were used to design the MSP antenna for ISM band application. Here the size of MSP was reduced and its useful for MIMO applications.

Keywords: Ferrites, Sol-gel, Electrical measurements, Magnetic measurements, Dielectric measurements.

1. Introduction

In these recent years, nano ferrite has an important application in developing the microwave device, high density information storage [1-2], various gas sensors [3], biological sensors [4] and three-dimensional color images [5]. There is an intensive research going on spinel ferrites with the formula MgFe_2O_4 . These ferrite shows a typical dielectric and magnetic properties. The saturation magnetization of these ferrites depends on Mg and Fe ratio [8], initially, there is an increase due to the imbalance on the Fe spin lattice and later it decreases due to the disruption of the Mg-Fe super exchange interactions [9]. To change the conductivity of these ferrites, a small amount of rare-earth elements was doped [10]. Various attempts have been made to study the effect of the rare-earth on spinel ferrites and found that the concentration of rare earth element ($x \leq 0.2$) leads to enhance the electric and magnetic behaviour [11-12]. Generally the rare-earth element has an unpaired electron in 4f shell which is completely shielded by 5s25p6. Here, the existence of 4f-3d coupling in these ferrites is due to the doping of the rare-earth element. As this coupling leads to the change in magneto crystalline anisotropy, affecting the electrical and magnetic properties [11] and strengthening the nanostructure ferrites compared to its bulk form. Obtain the desired electrical and magnetic properties in these ferrites by doping of different rare-earth the divalent elements in Mg/Fe site. However, the excellent hyperfine structure was obtained by the doping of two rare-earth elements in Fe site or two divalent elements in Mg site of this synthesized nano sized particle had been used to designing the MSP antenna. This MSP antenna had an application in ISM band [15] with high efficiency, high gain, high directivity, low loss, along with other

excellent antenna parameters. In this present investigation, an attempt has been made to synthesis Er-Dy doped MgFe₂O₄ ferrites and to study the structural, electrical and magnetic properties of the prepared ferrites. Here, the study of interest with respect to Er and Dy substituted in Mg ferrites lead to the higher magnetic entropy due to their elemental form. The characterization studies like X-ray diffraction (XRD), scanning electron microscopy (SEM), energy dispersive X-ray analysis (EDX), vibrating sample magnetometer (VSM), Four-probe electrical measurements, dielectric measurements were made on these as-prepared samples. The obtained results were discussed with its feasibility in terms of fabrication of MSP antenna.

2. Experimental

2.1. Synthesis of NanoFerrite Materials

Nanocrystalline powders MgEr_xDy_yFe_{2-x-y}O₄ were synthesized with the different composition of $x = 0.5, 0.8, 0.7$ and 0.9 and $y = 0.9, 0.7, 0.8$ and 0.5 employing the sol-gel combustion route with distilled water as a solvent [9, 13] and polyvinyl alcohol (PVA) was used as an agglomeration reduction agent [16]. The AR grade chemicals Citric acid (C₆H₈O₇.H₂O; Merck, India), ferric Nitrate [Fe (NO₃)₃.9H₂O] (Merck), Magnesium Nitrate [Mg (NO₃)₂.H₂O] (Lobo Chem.), Erbium Nitrate [Er (NO₃)₂. H₂O] (Alfa Aesar) and Dysprosium Nitrate [Dy (NO₃)₂.H₂O] (Alfa Aesar) were used for the present investigations without any further purification. The stoichiometric ratio of the base chemicals were weighed and mixed with deionized water under constant stirring. In order to obtain a solution with necessary pH value (between 7 and 8), ammonia solution was added with the stirring solution. During this process, the solution was stirred at 60°C. After the stabilization, the sol was kept at 80 °C for 24 hr. The obtained gel was ground and then heated at 200°C for 1h in an air furnace resulting in dark colored ash. The obtained ash powder was milled in agate mortar. Later, the prepared nano powders were sintered at 1200°C for 2h in a microwave furnace (MF/1600 °C/-21, VB Ceramics, India). The sintered ferrite particles were used for further characterization.

2.2 Physical parameter Studies

XRD Studies:

The phase composition analysis of fine ferrite powder was carried out using PAN analytical X' Pert Pro diffraction meter (the Netherlands) using Cu K α as a radiation ($\lambda = 1.54 \text{ \AA}$) source operating at a voltage of 40 kV and current rating of 30mA with a scanning rate of 0.01°/s and scan speed of 1°/min in a 2θ range of 10-80°. The crystallite size of the prepared samples was calculated employing by Scherrer's formula [7, 17].

Porosity:

The porosity of as-prepared ferrite samples was measured by the liquid displacement method (the Archimedes method) using CCl₄ as a buoyant. The weights of the sample in air and buoyant (W_a and W_b , respectively) were measured using a digital balance.

The measurement was taken ten times with different sizes of pellets to obtain the precise density value for each composition. The mean value of density was taken as the density of the sample.

Microscopic studies:

The obtained SEM images and the EDX patterns of the as-prepared samples were obtained employing scanning electron microscope (3000-H, Hitachi, Japan) to explore the morphology and the presence of chemical composition in the as-prepared ferrite nano powders.

Semiconductor Property Studies:

The electrical resistivity of the prepared ferrites was measured in the temperature range 283–563 K using standard four-probe method (DFM-RM, SES Instruments, India). The semiconducting properties of the prepared ferrites were obtained from the measured electrical resistivity in terms of various temperatures.

Electrical Measurements:

N4L LCR meter (PSM 1735, England) was used to undertake the dielectric measurements such as resistance, capacitance and loss tangent of the as-prepared ferrite samples. The experimental set-up for measuring the dielectric properties in the microwave region (0.1-20MHz) comprised of a pellet holder

connected to the N4L LCR meter interface with the computer. Dielectric properties were obtained with the help of this computer.

Magnetic Measurements:

The specific saturation magnetization (M_s), specific remanent magnetization (M_r) and the coercivity (HC) of the as-prepared nano ferrite powders were obtained using vibrating sample magnetometer (VSM 7410, Lake Shore, USA). The magnetometer was operated up to a maximum field of 10 kOe, in air at room temperature.

3. Results and Discussion

3.1 X-RAY Diffraction

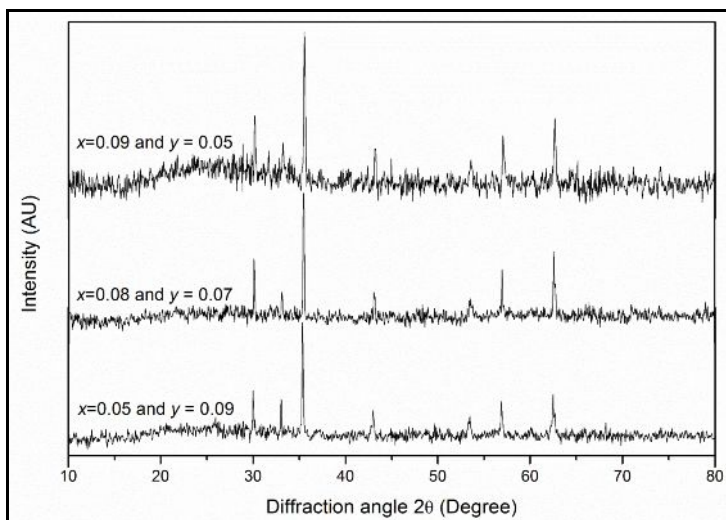


Fig.1 XRD patterns of $MgEr_xDy_yFe_{2-x-y}O_4$ with different Er and Dy content

Fig.1 shows the XRD patterns of the as-prepared nano ferrite samples. The observed peaks in XRD diffraction pattern reveal the crystalline nature of the samples. These observed peaks are well indexed with cubic spinel structure [18, 19 and JCPDS Nos: 89-3084, 20-0383 and 36-0964]. Further, the nano crystalline nature of the as-prepared ferrites confirms from the observed broader XRD diffracted peaks. However, the crystalline size of prepared these ferrites were obtained from full width at half maximum and diffraction angle employing the Scherrer formula.

Table 1 XRD- lattice constant and Particle size of $MgEr_xDy_yFe_{2-x-y}O_4$ ferrites

$MgEr_xDy_yFe_{2-x-y}O_4$		Lattice Constant	Grain size	Porosity
x	y	Å	nm	
0.05	0.09	8.37	43.29	0.297
0.07	0.08	8.41	46.75	0.317
0.09	0.05	8.44	43.29	0.326

The obtained values are mentioned in Table 1. It is inferred from Table 1 shows that the crystalline size of the ferrites increases with an increase in concentration of Er^{3+} and a decrease in concentration of Dy^{3+} ions. This may be due to the higher ionic radius of Er^{3+} than Dy^{3+} . There is a shift observed in the diffraction plane of (311) of this XRD pattern of the prepared ferrites. The decrease in diffraction angle for diffraction plane (311) is due to increase in concentration of Er^{3+} or a decrease in concentration of Dy^{3+} . Further, the lattice constant of the spinel structure was calculated for the prominent (311) diffracted plane employing the standard relation discussed in literature [9]. The obtained lattice constant is given in Table 1 along with the crystalline size for easy comparison. It is evident from Table 1 shows that the lattice constant increases with an increase in concentration of Er^{3+} . The porosity of the ferrites increases with an increase in concentration of

Er³⁺. The measured porosity of the ferrites by liquid displacement method is given in Table 1. Thus, the single phase cubic Erbium and Dysprosium substituted magnesium ferrite nano crystals was successfully synthesized by sol-gel combustion technique, without any secondary phases.

3.2 EDX

EDX pattern obtained for MgEr_xDy_yFe_{2-x-y}O₄ samples is shown in Figs. 2-5. The EDX spectra of the as-prepared ferrites comprises of Mg, Er, Dy and Fe. The estimated weight percentage of the constitute elements are in close agreement with the starting stoichiometric ratio of the as-prepared ferrites. Thus, it reveals the purity of the as-prepared ferrites. The no trace detected for other elements in EDX spectra confirms the purity of the prepared ferrites.

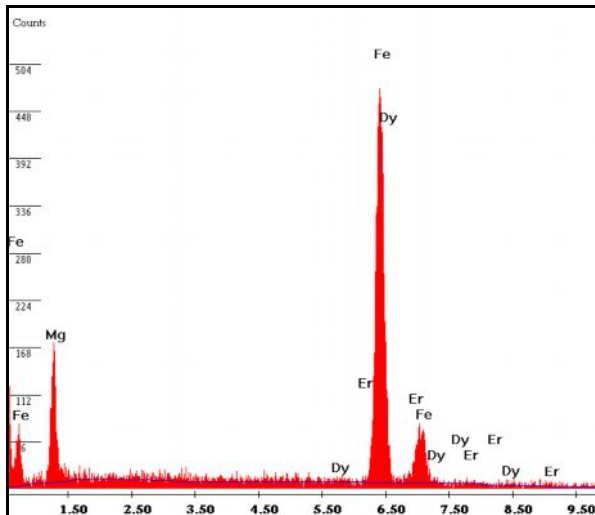


**Fig.2 EDAX of MgEr_xDy_yFe_{2-x-y}O₄
= 0.05 y = 0.09**

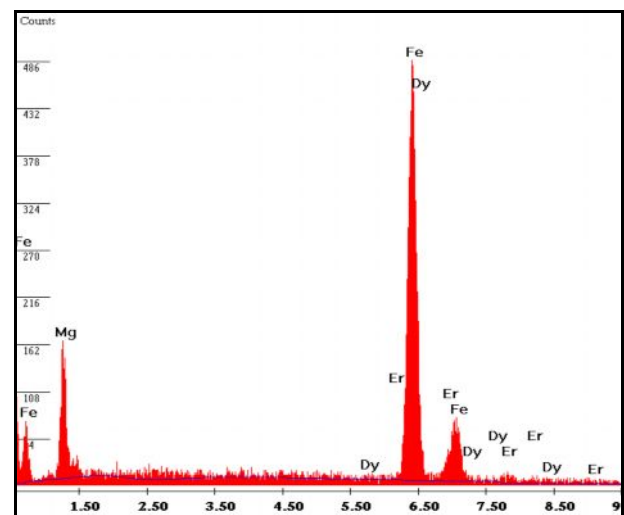
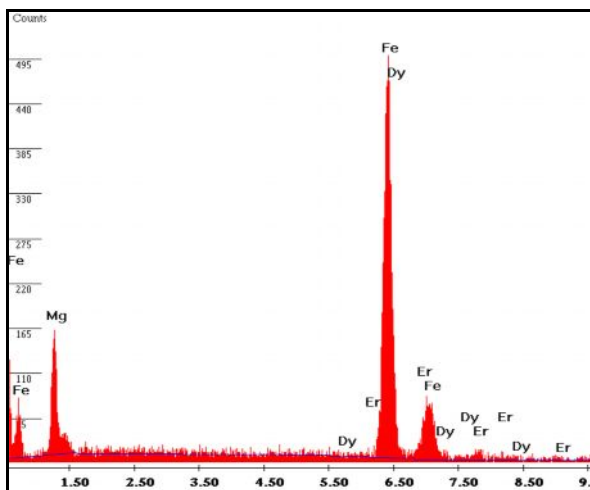


Fig.3 EDAX of MgEr_xDy_yFe_{2-x-y}O₄ x = 0.07 y = 0.08



**Fig.4 EDAX of MgEr_xDy_yFe_{2-x-y}O₄
= 0.08 y = 0.07**

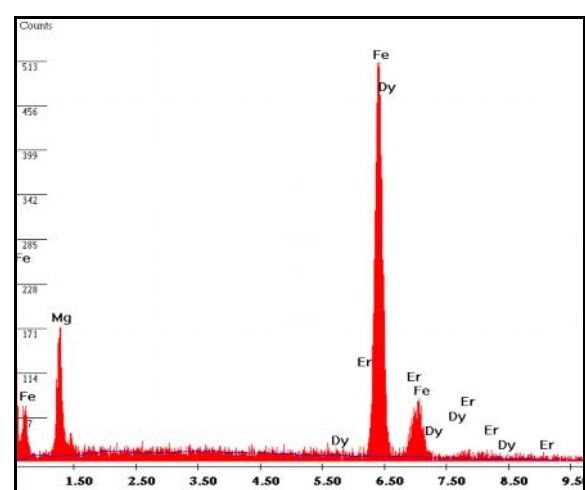


Fig.5 EDAX of MgEr_xDy_yFe_{2-x-y}O₄ x = 0.09 y = 0.05

3.3 SEM Analysis

The SEM image of MgEr_xDy_yFe_{2-x-y}O₄ samples is shown in Figs. 6-9. The SEM images reveal that the particles are highly porous and spherical like morphology. The particles are highly agglomerated in nature. It is difficult to obtain the exact particle size from these SEM images.

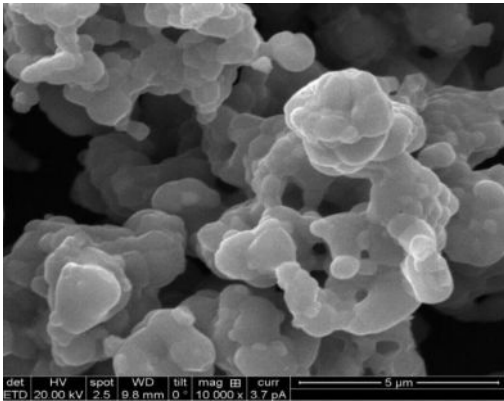


Fig.6 SEM of MgEr_xDy_yFe_{2-x-y}O₄ x = 0.05 y = 0.09

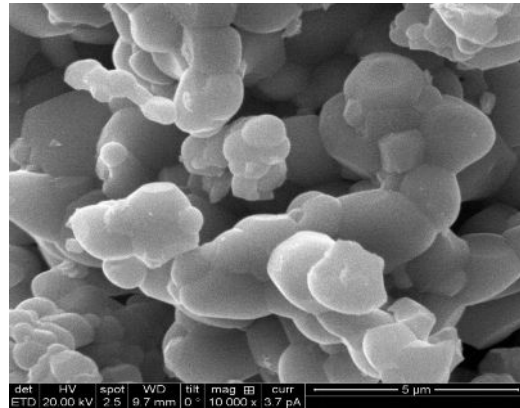


Fig.7 SEM of MgEr_xDy_yFe_{2-x-y}O₄ x = 0.07 y = 0.08

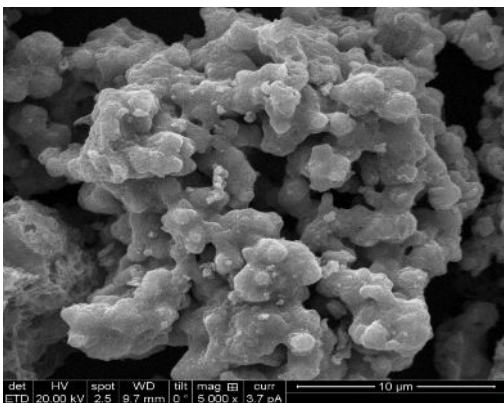


Fig.8 SEM of MgEr_xDy_yFe_{2-x-y}O₄ x = 0.08 y = 0.07

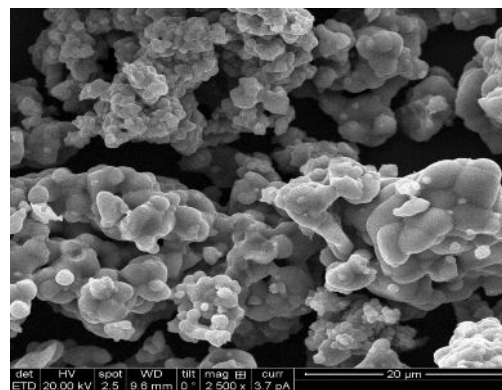


Fig.9 SEM of MgEr_xDy_yFe_{2-x-y}O₄ x = 0.09 y = 0.05

However, the average particle size of the prepared ferrites is obtained by considering the maximum and minimum numbers of the ferrite particles. The average particle size range obtained for MgEr_{0.05}Dy_{0.09}Fe_{1.86}O₄, MgEr_{0.07}Dy_{0.08}Fe_{1.85}O₄, MgEr_{0.08}Dy_{0.07}Fe_{1.85}O₄ and MgEr_{0.09}Dy_{0.05}Fe_{1.86}O₄ are respectively 0.25-1.0, 0.64-1.5, 0.80-2.5 and 1.4-3.0μm. Further, the particle size of the ferrites increases with an increase in concentration of Er³⁺. This measurement is in line with earlier XRD studies.

3.4 Semiconductor Property

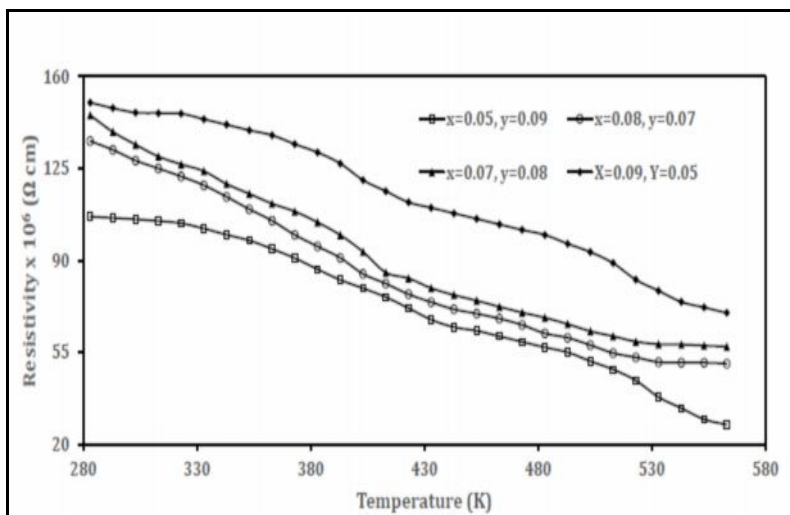


Fig.10 Temperature dependent Resistivity of MgEr_xDy_yFe_{2-x-y}O₄ ferrites

Four probe was used to study the temperature dependence of electric resistivity of the prepared $\text{MgEr}_x\text{Dy}_y\text{Fe}_{2-x-y}\text{O}_4$ ferrites. It is seen that the voltage showed a fall with an increase in temperature (from 283 to 563 K) shown in Figure 10. The above observations conclude that the as-prepared $\text{MgEr}_x\text{Dy}_y\text{Fe}_{2-x-y}\text{O}_4$ ferrites behave as an n-type material between this temperatures range [20-22]. This conduction in nano structured Mg Ferrite doped with Er and Dy showed the polaron hopping conduction [9, 21]. The incorporation of Mg^{2+} , Er^{3+} and Dy^{3+} ions takes place into the tetrahedral sites [22-24]. Since, the DC resistivity decreases as a function of temperature; it shows the semiconducting nature in the ferrites. The positive value of Seebeck coefficient establishes n-type conduction behaviour [21]. Further, it is seen that the room temperature resistivity of the prepared ferrite samples is more than around $\sim 10^6 \times 10^6 \Omega \text{ cm}$. It is also seen that the resistivity decreases with increasing the concentration of Er^{3+} and a decrease in concentration of Dy^{3+} in $\text{MgEr}_x\text{Dy}_y\text{Fe}_{2-x-y}\text{O}_4$ ferrites. Generally, it is reported that in the polycrystalline ferrites show that the bulk resistivity rises from the combination of crystallite resistivity and the resistivity of crystallite boundaries [24-26]. Since, the boundary resistivity is much greater than that of the crystallite resistivity; the boundary has a greater influence on the dc resistivity. The decrease of resistivity is also related to the decrease of porosity. The pores are non-conductive which increases resistivity of the material [21]. The resistivity decreases with the decrease of porosity because charge carriers on their way face the pores. It is seen that the decrease in dc resistivity with an increase in concentration of Er^{3+} and a decrease in concentration of Dy^{3+} in $\text{MgEr}_x\text{Dy}_y\text{Fe}_{2-x-y}\text{O}_4$ ferrites is observed. It is also reported that the activation energy decreases with increasing grain size of the particle. It is inferred from earlier XRD and SEM measurements that the crystalline size of the ferrites increases with an increase in concentration of Er^{3+} and a decrease in concentration of Dy^{3+} , as its reported that the decrease in activation energy with the increase in concentration of Er^{3+} and a decrease in concentration of Dy^{3+} may attributed to the fact that partial reduction of Fe^{3+} to Fe^{2+} which takes place locally and thus, these places act as donor center [8, 11 19]. In ferrite samples, the activation energy is also associated with the variation of mobility of charge carriers rather than with their concentration [19]. The charge carriers are considered to be localized at the ions or vacant sites and thus conduction occurs via a hopping process. Since, the hopping depends upon the activation energy, which in turn is associated with the electrical energy barrier experienced by these electrons [26-28]. Thus, the conduction mechanism is occurring here due to the hopping of electrons from the Fe^{3+} type to Fe^{2+} type. The higher value of dc resistivity is due to the inclusion of rare-earth content in Mg ferrite. The rare-earth doping reduces the Fe ion concentration from 2 to 1.85 thereby reduces the number of Fe^{3+} ions on the octahedral sites which play a dominant role in the mechanism of conduction [18]. It is also seen that the resistivity of the sample decreases with increase in temperature according to Arrhenius equation [17, 18, 29-30], which shows that the increase in temperature leads to decrease in resistivity, which is in accordance to the normal behaviour of n type semiconducting materials. Thus, the increase in temperature of the sample will help the trapped charges to be liberated and allow them to participate in the conduction process, resulting into the decrease of the resistivity. This decrease in resistivity is used to explain the increase in the drift mobility of the thermally activated electrons according to the hopping conduction mechanism and not due to the thermally creation of the charge carriers. Here, the hopping conduction mechanisms between $\text{Fe}^{2+} \leftrightarrow \text{Fe}^{3+} + e^-$ will act as a main source of electron hopping.

3.5 Hysteresis

The vibrating sample magnetometer was used to obtain the magnetic measurements of the as-prepared ferrites shown in Figure 11. The obtained saturation magnetization, coercivity and remanent magnetization from hysteresis loops at room temperature are listed in Table 2. The obtained saturation magnetization (M_s) at room temperature is found to be 29-32 emu/g and remnant magnetization (M_r) is 8-12 emu/g. The obtained values for M_s and M_r of lanthanide doped ferrites are greater than the earlier reported values for MgFe_2O_4 ferrites [19-22, 24]. Since, the magnetic moment of Er^{3+} and Dy^{3+} ions is much greater than Fe^{3+} ions, a replacement of Fe^{3+} ions by Er^{3+} or Dy^{3+} ions at B site results an magnetic moment increases. The increase in saturation magnetization was observed with an increase in concentration of Er^{3+} and a decrease in concentration of Dy^{3+} ions. The increase in magnetization of the prepared ferrites may explained by annihilation of a nonmagnetic layers (surface dead layers) due to the lanthanide doping. The coercivity of the prepared ferrites strongly depends on the particle size and anisotropy of the materials. In multi-domain particles, the magnetization reversal occurs due to the domain wall movement. As the domain walls move through a particle, they are pinned at grain boundaries. The additional energy is required for domain walls to continue the wall movement. Therefore, the doping of lanthanides creates more pinning sites and increases the coercivity of the ferrites. In the present investigation, the observed super-paramagnetic behaviour in $\text{MgEr}_x\text{Dy}_y\text{Fe}_{2-x-y}\text{O}_4$ ferrite nanoparticles attributes to spin canting and surface spin disorder which occurred in these nano crystallized particles [19, 20, 22]. These observed values for M_s and M_r of lanthanide doped ferrites suggest their suitability in applications like magnetic targeting and separators [22].

Table 2 Magnetic saturation, retentively, coercive force of MgEr_xDy_yFe_{2-x-y}O₄ ferrites

S. No	Mg Er _x Dy _y Fe _{2-x-y} O ₄		Coercivity (G)	Remanence (emu/g)		Saturation Magnetization (emu/g)		Retentivity (emu/g)
	x	y		Positive	Negative	Positive	Negative	
	1	0.05		0.09	334.23	7.1119	-7.0139	
2	0.07	0.08	332.98	10.543	-10.565	27.066	-27.062	10.554
3	0.07	0.08	333.07	10.754	-10.602	28.166	-28.132	10.678
4	0.09	0.05	335.88	12.823	-12.617	32.032	-32.022	12.720

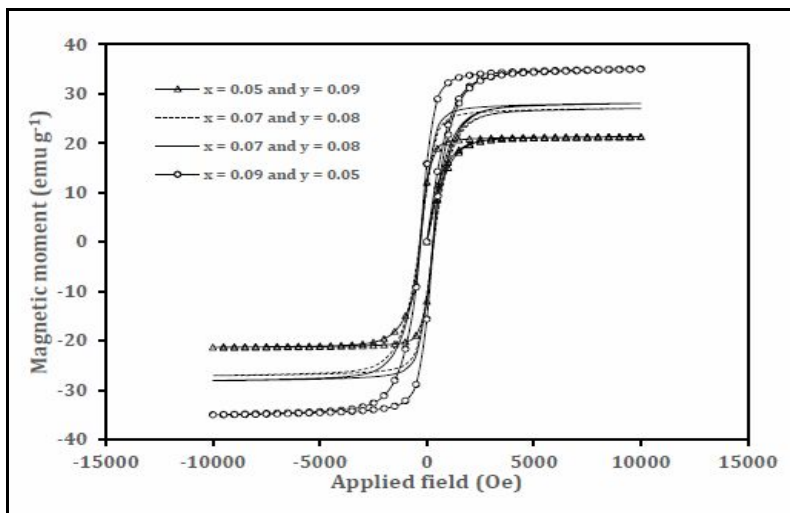


Fig. 11 Hysteresis loop of MgEr_xDy_yFe_{2-x-y}O₄ ferrites

3.6 Electrical Properties

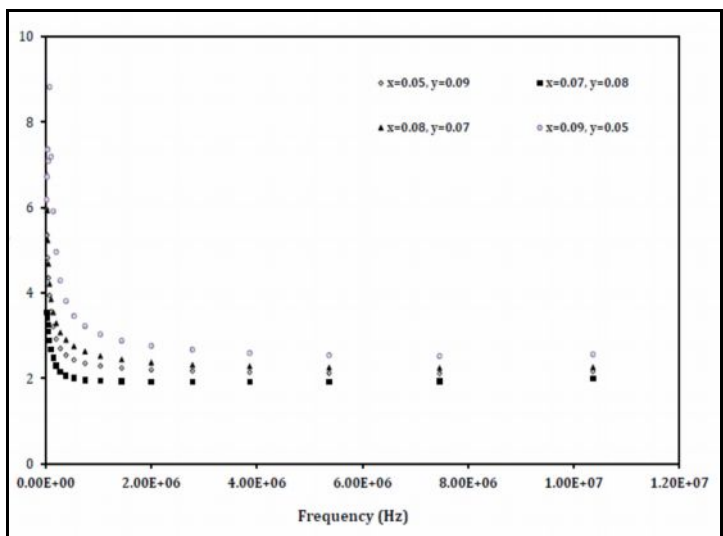


Fig. 12 Variation of dielectric constant of MgEr_xDy_yFe_{2-x-y}O₄ ferrites with frequency

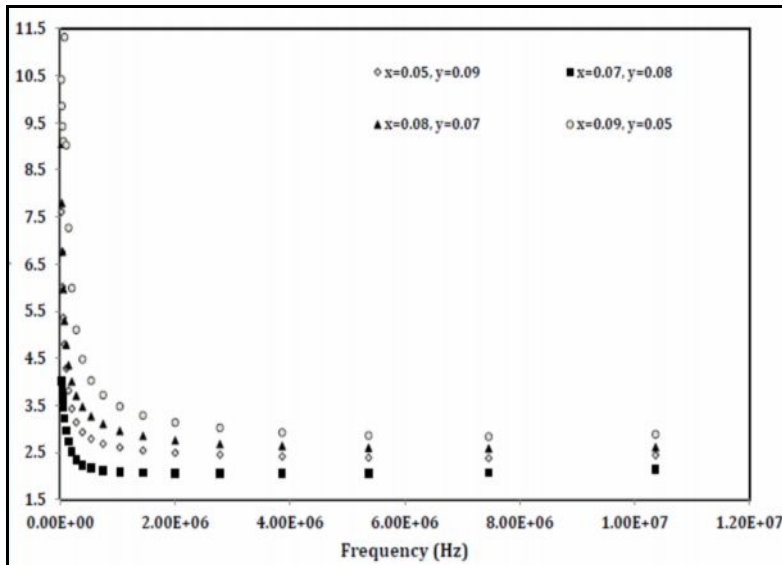


Fig. 13 Variation of absolute permittivity of MgEr_xDy_yFe_{2-x-y}O₄ ferrites with frequency

Figs. 12 and 13 show the variation of dielectric constants of ferrite MgEr_xDy_yFe_{2-x-y}O₄ samples at different frequencies. At lower frequencies (100 kHz), the dielectric constant is very large, while at higher frequency (2–10MHz), the dielectric constant reduces and becomes linear. It has been seen that for the large value of dielectric constants leads to a large dielectric polarization. The higher value of dielectric constant of the material leads to higher value of polarization. There are four key mechanisms causing polarizations: electronic, ionic, dipolar and space charges polarization. Their occurrence depends upon the electric frequency of the applied field [21, 31-32]. It is seen that at low frequencies, space charges polarization and dipolar polarization are known to play the vital role [31-33] and both of these polarizations are temperature dependent. Whereas at high frequencies, ionic polarizations is mainly contributes due to their insignificant with temperature. It is found that the maximum and minimum value of dielectric constant is 30.963 and 1.172 respectively for MgEr_xDy_yFe_{2-x-y}O₄ ferrites. The maximum and minimum value of the dielectric values are respectively 2.01 and 2.585 ($x=0.05$ and $y=0.09$), 2.96 and 3.785 ($x=0.07$ and $y=0.08$), 2.98 and 2.584 ($x=0.08$ and $y=0.07$) and, 3.12 and 8.81 ($x=0.09$ and $y=0.05$). The dielectric loss follows the same trend as the dielectric constant curves, and this is explained on the similar to dielectric constant. The low values of dielectric constant, dielectric loss and high value of dc resistivity are due to the rare-earth ion content in Mg ferrite. This result is explained in view of the hopping conduction mechanism between $Fe^{2+} \leftrightarrow Fe^{3+} + e^{-}$, as rare-earth ions do not participate in conduction and polarization process which limit the degree of hopping by blocking up $Fe^{2+} \leftrightarrow Fe^{3+} + e^{-}$ pattern on the octahedral sites [21, 32- 34]. This is due to the reduction in the concentration of Fe ions in the system due to the doping of rare-earth ions in Mg ferrite [33, 35].

4. Conclusion

In the present studies, sol-gel route was found to be simple and efficient for the synthesis of Er, Dy doped Magnesium ferrites. The nanocrystalline MgEr_xDy_yFe_{2-x-y}O₄ ferrite powders were successfully synthesized with different doping. The phase purity, crystallite size and particle size of the prepared ferrites was confirmed by XRD and SEM micrographs. Semiconducting behaviour of the ferrites was confirmed by using temperature-dependent resistivity measurements. The magnetic saturation, coercivity and remanent of the as-prepared ferrites was obtained by analyzing the hysteresis curves. The dielectric constant and loss tangent of the ferrites were determined by using LCR meter. It is found that the maximum and minimum value of dielectric constant for MgEr_xDy_yFe_{2-x-y}O₄ ferrites is 8.81 and 2.01 respectively. From the above features it may be concluded that the prepared ferrites samples are the suitable candidate material for designing the MSP antenna.

Acknowledgement

The authors are thankful to Defence Research Development Organization (DRDO), New Delhi for the finical support to carry out this work (ERIP/ER/1104637/M/01/481, Dated 20.06.2013).

References

1. E.Melagiriappa, H.S Jayanna and B.K Chougule, *Mater. Chem. Phys.*112 (2008) 68-73.
2. Z.Yue, L. Li, J.Zhou, H.Zhang and Z. Gu, *Mater. Sci.Engg B64* (1999) 68-72.
3. E.V Groman, J.C Bouchard, C.P Reinhardt and D.E Vaccars, *Bioconjugate Chem.* 18 (2007) 1763-71.
4. J.Wang, J.Zhou, Z.Li, Y.Song, Q.Liu, Z.Jiang and M.Zhang, *Chem. - A European J.* 16 (2010) 14404-414.
5. S.S Jadhav, S.M Patange and K.M Jadhav, *Journal of Biomedical and Bioengineering*, 1 (2010) 21-29.
6. E. Ateia, *Egypt. J. Solids*, 29(2006) 317-327.
7. R.Iyer, R. Desai and R.V Upadhyay, *Indian J Pure Appl.Phys*,49 (2009) 180.
8. A. Pradeep and G. Chandrasekaran, *Mat. Lett.*60 (2006) 371-374.
9. A. Pradeep, P. Priyadharsini and G.Chandrasekaran, *J. Magn. Magn. Mater.* 320 (2008) 2774-2779
10. A.F Rawle, *Powder Technology*, 174 (2007) 6-9.
11. M.Z Said, D.M Hemed, S .Abdel Kader and G.Z Farag, *Turk. J. Phys.* 37 (2007) 41-50.
12. A.A Sattar and K.M El-Shokrofy, *Phys. IV France* 07 (1997) C1-245-246
13. G.Kumar, S.Sharma, R.K. Kotnala, J.Shah, S.E Shirsath, K.M Batoo and M.Singh, *J.Molecular Structure*, 1051 (2013) 336-344.
14. C.P Liu, M.W Li, Z.Cui, J.R Huang, Y.LTian, T.Lin and W.B Mi, *J. Mater. Sci.* 42 (2007) 6133-6138.
15. G.M Bhongale, V.B Sapre and D.K Kulkarni, *Bull.Mater. Sci.* 16 (1993) 243-253.
16. M.K. Shobana, H.Kwon and H.Choe, *J. Magn. Magn. Mater.*324 (2012) 2245-2248.
17. K.Sakthipandi and V.Rajendran, *Mater. Chem.Phys.* 138 (2013) 581-592.
18. A.B Gadkari, T.J Shinde and P.N Vasambekar, *J. Mater.Sci.: Mater. Elect.* 21 (2010) 96-103.
19. J.Chand, G.Kumar, P.Kumar, S.K Sharma, M.Knobel and M.Singh, *J. Alloys Compd.* 486 (2009) 376-379.
20. A.BGadkari, T.JShinde and P.N Vasambekar, *Rare Metals*, 29 (2010) 168-173.
21. A.B Gadkari, T.J Shinde and P.N Vasambekar, *J. Magn. Magn. Mater.*322 (2010) 3823-3827.
22. V Naidu, S.K.A.A.K Sahib, M.Suganthi and C Prakash, *Inter. J. Comp.Appl.* 27 (2011) 18-22.
23. J. Chandradass, H.Kim and Francis W.Y Momade, *J. Sol-Gel Sci.Tech.*65 (2013) 189-194.
24. G.Dascalu, T.Popescu, M.Feder and O.F Caltun, *J. Magn. Magn. Mater.*333, (2013) 69-74.
25. M.Kumar and K.L Yadav, *J. Phys.Condens. Matt.* 19 (2007) 242202.
26. D.H Wang, W.C Goh, M.Ning and C.Kong, *Appl. Phys. Lett.* 88(2006) 212907.
27. S.Yamada and E. Otsuki, *J. Appl. Phys.* 81 (1997) 4791.
28. N.M Deraz and A.Alarifi, *Int. J. Electrochem. Sci.* 7 (2012)6501 - 6511.
29. P K Roy and J Bera, *Mater. Res. Bull.*(2007) 77-83.
30. C.Venkataraju, *Appl. Phys. Res.* 1 (2009) 41-45.
31. L.E Hollander and P.L Castro, *J.Appl. Phys.* 33(1962) 3421.
32. D.M Eagles and M.Georgiev and PC Petrova, *Phys. Rev.B* 54 (1996) 22-25.
33. J.Zhao, S.Liu, W.Zhang, Z.Liu and Z.Liu, *J. Nanopart. Res.* 15 (2013) 1969.
